SCIENCE CHINA
Technological Sciences

• Article •

January 2023 Vol. 66 No. 1: 243–254
https://doi.org/10.1007/s11431-022-2172-8

A network-based virtual slack bus model for energy conversion units in dynamic energy flow analysis

HUANG YuJia, SUN QiuYe*, WANG Rui & LIU GuangLiang

School of Information Science and Engineering, Northeastern University, Shenyang 110819, China

Received May 4, 2022; accepted August 8, 2022; published online December 26, 2022

Integrated energy system (IES) is a viable route to "carbon peak and carbon neutral". As the basis and cornerstone of economic operation and security of IES, energy flow calculation (EFC) has been widely studied. Traditional EFC focuses on the single or distributed slack bus models, which results in the lack of unlimited power to maintain system operation, especially for electric power grid working in islanded or coupled mode. To deal with this problem, this paper proposes a network-based virtual-slack bus (VSB) model in EFC. Firstly, considering the anticipated growth of energy conversion units (ECUs) with power adjustment capacity, the generators and ECUs are together modeled as a virtual slack bus model to reduce the concentrated power burden of IES. Based on this model, a power sensitivity method is designed to achieve the power sharing among the ECUs, where the power can be allocated adaptively based on the network conditions. Moreover, the method is helpful to maintain the voltage and pressure profile of IES. With these changes, a dynamic energy flow analysis including virtual slack bus types is extended for IES. It can realize the assessment of the system state. Finally, simulation studies illustrate the beneficial roles of the VSB model.

integrated energy system, energy flow analysis, power sensitivity method, virtual slack bus

Citation: Huang Y J, Sun Q Y, Wang R, et al. A network-based virtual slack bus model for energy conversion units in dynamic energy flow analysis. Sci China Tech Sci, 2023, 66: 243–254, https://doi.org/10.1007/s11431-022-2172-8

1 Introduction

With the increasing contradiction between the demand for energy in industrial production and residential life and environmental friendliness, energy reform technologies represented by "carbon peak and carbon neutral" [1] and "multi-energy interconnection" have become the key development direction of science and technology strategy. Electric power, as an industry with the highest carbon emissions, has become an inevitable choice to replace traditional fossil energy power generation with "zero carbon emissions" new energy and low-carbon emission based gas power generation [2]. This also makes the integrated energy system (IES) [3] with electricity, gas and heat as the main energy carrier and their internal coupling relationship increasingly complex. Therefore, in-depth study on collaborative analysis of multi-energy systems has become an inevitable trend [4].

Energy flow calculation (EFC), as the cornerstone of IES studies, calculates state variables such as nodal voltage/pressure/temperature, and line transmission flow in IES based on limited known information. The EFC results are helpful for judging whether or not the system state is within the operating limits. Moreover, the obtained results can provide initial operating conditions for high-level research on IES, such as planning and optimization [5]. In summary, the EFC is of great significance to IES.

Traditional energy flow analysis for electric power grid (EPG) uses a single slack bus (SSB), which is generally applicable to large-scale interarea power systems or small grid-connected systems [6]. However, for the EPG working in islanded mode or coupled mode, the SSB cannot provide un-

*Corresponding author (email: sunqiuye@ise.neu.edu.cn)

© Science China Press and Springer-Verlag GmbH Germany, part of Springer Nature 2022

limited and sufficient power to match the total system load plus power losses. This may exceed the rating of certain generators and result voltage profile collapse [7]. To address the issue, a distributed slack bus (DSB) concept was proposed. The total active power imbalance in EPG is shared among each generator based on their participation factors. In ref. [8], a participation factor selected method for distribution power system was proposed. The method is related to generator domains and can reflect the capacities of distributed generators. In ref. [9], the participation factors based on optimization criteria were proposed to share the total active power losses. In ref. [10], a sequence frame-based distributed slack bus model considering power limit violation was proposed. These work focus on the distribution power systems that work independently, may not be suitable for EPG coupled with natural gas network (NGN) and district heating network (DHN). For example, the main generators of EPG in coupled mode are gas-fired power generations (GPG) or combined heat and power (CHP) units. The capacity of GPG and CHP units are mainly decided by the volume flow extracted from the NGN. However, the gas-based unit varies its volume flow consumptions to balance the total active power, which leads to the pressure fluctuations in NGN and impacts both reliability and safety of IES [11, 12].

To overcome the shortcoming that the existing slack bus model is not suitable for EPG in coupled model, ref. [13] considered rapid response ability of GPG in peak regulation, and firstly used the distributed slack bus model with constant participation factors for GPG in EFC. On this basis, ref. [14] added the influence of DHN. Ref. [15] proposed a multi-slack bus model for both NGN and EPG in EFC. The model is more accurate compared with the traditional SSB model. Ref. [12] introduced multiple slack nodes to overcome the shortcoming of adjusting active power by a single GPG unit, which avoids the suffering of calculation accuracy in coupled system with large wind power fluctuation. Ref. [16] proposed a multi-slack bus model in EFC for coupled system with bi-directional energy conversion. The model integrated the fast power adjustment ability of GPG and power-to-gas (P2G) units, and had more practical significance. These work had achieved the power balance by slack buses based on constant participation factors or optimization criteria. However, in practice, the network topology and system condition play a critical role in the participation of generators in serving loads and losses. On the other hand, the mentioned above based on the steady-state models of IES [12–16]. The models do not consider the slow dynamic characteristics of the NGN and DHN [17], leading to an incomplete and inaccurate assessment of IES. As a result, the flexibility of IES cannot be fully exploited, which is contrary to the motivation of deploying IES [18].

Therefore, to efficiently and accurately solve the active power balance problem of IES, this paper proposes a network-based virtual slack bus model for EFC in IES considering the slow dynamic. The main contributions of this paper are summarized as follows.

(1) The generators and energy conversion units (ECUs) in IES with power adjustment capacity are modeled as virtual slack buses (VSB), which can effectively share the load along with physical slack. By this way, the concentrated burden of IES is removed.

(2) For the foresaid VSB model, a power sensitivity method is designed to achieve the power sharing among the ECUs. This method not only adaptively allocates the power based on the network conditions, but also is helpful to maintain the voltage and pressure profile of IES.

(3) Based on the proposed VSB model, the bus types are reclassified for coupled power grid. Then, a dynamic energy flow analysis including VSB is extended to realize the system state assessment of IES and stable operation analysis.

This paper is organized as follows: the virtual slack bus model based on power sensitivity analysis is described in Sect. 2. The dynamic energy flow analysis with VSB model is formulated in Sect. 3. Finally, several case studies are carried out on typical systems in Sect. 4, and conclusions are given in Sect. 5.

2 Network-based virtual slack bus model for energy conversion units

The virtual slack bus model in this paper mainly takes into account the advantage of energy conversion units in adjusting active power based on the power sensitivity method. It enables each energy conversion unit with the functionality of power adjustment ability as a virtual slack bus. Consequently, the reference slack bus and the virtual slack buses work together to compensate the active power imbalance.

Assuming that the number of total buses for the electricity power grid is N_e, the nodal active power mismatches ΔP_i and reactive power mismatches ΔQ_i equations are given by

$$\Delta P_i = P_i - \sum_{j=1}^{N_e} |V_i||V_j|(G_{ij}\cos\theta_{ij} + B_{ij}\sin\theta_{ij}), \tag{1}$$

$$\Delta Q_i = Q_i - \sum_{j=1}^{N_e} |V_i||V_j|(G_{ij}\sin\theta_{ij} - B_{ij}\cos\theta_{ij}), \tag{2}$$

where P_i and Q_i are the scheduled active and reactive power values injected into bus i, respectively. $|V_i|$ and $|V_j|$ are voltage magnitudes of bus i and j while θ_{ij} is the difference of voltage angles i and j. G_{ij} and B_{ij} are electricity conductance and susceptance of transmission line ij, respectively.

By applying Taylor series expansion to eqs. (1) and (2) while neglecting higher-order terms, the initial equation can be obtained as follows:

$$\begin{bmatrix} \boldsymbol{\Delta\theta} \\ \boldsymbol{\Delta V} \end{bmatrix} = \boldsymbol{J}^{-1} \begin{bmatrix} \boldsymbol{\Delta P} \\ \boldsymbol{\Delta Q} \end{bmatrix} = \begin{bmatrix} \boldsymbol{H}^{11} & \boldsymbol{H}^{12} \\ \boldsymbol{H}^{21} & \boldsymbol{H}^{22} \end{bmatrix} \begin{bmatrix} \boldsymbol{\Delta P} \\ \boldsymbol{\Delta Q} \end{bmatrix}, \tag{3}$$

where $[\boldsymbol{\Delta\theta}, \boldsymbol{\Delta V}]^{\mathrm{T}}$ are the vectors of voltage mismatches. $\boldsymbol{J}$ is Jacobin matrix consisting of the partial derivatives of P and Q to θ and V, respectively. The matrix of $\boldsymbol{J}^{-1}$ is defined as $\boldsymbol{H}$, in which $\boldsymbol{H}^{11}$, $\boldsymbol{H}^{12}$, $\boldsymbol{H}^{21}$, $\boldsymbol{H}^{22}$ are the submatrices. Since the exchange active power of energy conversion units is always the focus, the mismatches ΔP_i are separated into active power contribution $\Delta P_i^{\mathrm{vsb}}$ and load mismatches $\Delta P_i^{\mathrm{load}}$ at virtual slack buses. Consequently, the active power and voltage angle mismatches in virtual slack buses can be written as

$$\begin{bmatrix} \Delta\theta_2 \\ \vdots \\ \Delta\theta_{N_s} \end{bmatrix} = \boldsymbol{S}_1 \begin{bmatrix} \Delta P_2^{\mathrm{vsb}} \\ \vdots \\ \Delta P_{N_s}^{\mathrm{vsb}} \end{bmatrix} + \boldsymbol{S}_2 \begin{bmatrix} -\Delta P_2^{\mathrm{load}} \\ \vdots \\ -\Delta P_{N_s}^{\mathrm{load}} \\ \vdots \\ \Delta P_{N_e} \\ \vdots \\ \Delta Q \end{bmatrix}, \tag{4}$$

where N_s is the number of slack buses (N_s-1 virtual slack buses and one reference bus). $\boldsymbol{S}_1$ and $\boldsymbol{S}_2$ are submatrices made up of the elements in $\boldsymbol{H}$. $\boldsymbol{S}_1$ and $\boldsymbol{S}_2$ are expressed by

$$\boldsymbol{S}_1 = \begin{bmatrix} H_{2,2}^{11} & \cdots & H_{2,N_s}^{11} \\ \vdots & \ddots & \vdots \\ H_{N_s,2}^{11} & \cdots & H_{N_s,N_s}^{11} \end{bmatrix}, \tag{5}$$

$$\boldsymbol{S}_2 = \left[\begin{array}{ccc|ccc} H_{2,2}^{11} & \cdots & H_{2,N_e}^{11} & H_{2,2}^{12} & \cdots & H_{2,N_e}^{12} \\ \vdots & \ddots & \vdots & \vdots & \ddots & \vdots \\ H_{N_s,2}^{11} & \cdots & H_{N_s,N_e}^{11} & H_{N_s,2}^{12} & \cdots & H_{N_s,N_e}^{12} \end{array}\right], \tag{6}$$

where subscripts denote elements of J^{-1}. Since the voltage and phase angle mismatches are zero in the ideal state [19], eq. (4) can be written as

$$\begin{bmatrix} \Delta P_2^{\mathrm{vsb}} \\ \vdots \\ \Delta P_{N_s}^{\mathrm{vsb}} \end{bmatrix} = -[\boldsymbol{S}_1]^{-1}\boldsymbol{S}_2 \begin{bmatrix} -\Delta P_2^{\mathrm{load}} \\ \vdots \\ -\Delta P_{N_s}^{\mathrm{load}} \\ \vdots \\ \Delta P_{N_e} \\ \vdots \\ \Delta Q \end{bmatrix}. \tag{7}$$

Therefore, the power sensitivity of virtual slack buses with respect to load changes can be represented by the power sensitivity matrix

$$\boldsymbol{S} = -[\boldsymbol{S}_1]^{-1}\boldsymbol{S}_2. \tag{8}$$

Through the power sensitivity matrix, we can calculate the power contribution of each unit corresponding to the load mismatches. It is worth noting that changes in renewable energy sources injection ΔP^{RES} can be regarded as negative load, that is $-\Delta P^{\mathrm{load}}$. The power sensitivity method obtains the variation state of the power through the internal differential relation of the Jacobian matrix.

Finally, the scheduled active power P_i at virtual slack bus i is updated by

$$P_i^{\mathrm{vsb}} = P_i^{\mathrm{vsb},0} + \Delta P_i^{\mathrm{vsb}}, \tag{9}$$

where $P_i^{\mathrm{vsb},0}$ is the set-point of active power of unit at bus i.

The combined heat and power (CHP) and GPG units with rapid response ability are widely used as generators in IES. When the GPG or CHP units are modelled as virtual slack buses, eq. (9) can be expressed as

$$P_i^{\mathrm{GPG/CHP}} = P_i^{\mathrm{GPG/CHP},0} + \Delta P_i^{\mathrm{GPG/CHP}}, \tag{10}$$

where P_i^{GPG} and P_i^{CHP} are the generated active power of GPG and CHP units.

Similarly, the electric load P2G and electric boilers (EB) units are widely used for electric power adjustment due to their great flexibility [20,21]. They can be considered as negative generators. When the P2G or EB units are modelled as virtual slack buses, eq. (9) can be expressed as

$$-P_i^{\mathrm{P2G/EB}} = -P_i^{\mathrm{P2G/EB},0} + \Delta P_i^{\mathrm{P2G/EB}}, \tag{11}$$

where P_i^{P2G} and P_i^{EB} are the consumed active power of P2G and EB units.

Then the power output or input of energy conversion units P_i^{GPG}, P_i^{CHP}, P_i^{P2G} and P_i^{EB} are regulated according to their assigned active power slack $\Delta P_i^{\mathrm{vsb}}$ based on the power sensitivity matrix $\boldsymbol{S}$. With the virtual slack bus model in this paper, all the energy conversion units with power adjustment ability instead of the single traditional generator, participate in power adjustment through $\Delta P_i^{\mathrm{vsb}}$.

Remark 1: According to eqs. (7)–(11), with the virtual slack bus model in this paper, all the energy conversion units with power adjustment ability instead of the traditional gas-fired generator at single reference bus in IES, participate in power adjustment through $\Delta P_i^{\mathrm{vsb}}$. This is helpful to remove the concentrated burden on single reference bus, thus reducing the impact on the primary side gas network. In addition,

the P2G and EB units are modeled as negative generation units to act as virtual slack buses in eq. (11), which helps to improve the system's power fluctuation accommodation capacity by releasing or increasing the units input power. Finally, the calculated power of each unit at virtual slack bus is updated with the power sensitivity matrix $\boldsymbol{S}$, which adaptively changes with the network parameters and system conditions.

3 Implementation of the VSB model in energy flow formulation of IES

Based on the proposed VSB model, a power flow model with new bus types definition is formulated in Sect. 3.1. Since the VSB solves the power imbalance and limited power capacity of electric network with ECUs, the ECUs models are introduced in Sect. 3.2. Next, considering the operation of ECUs will affect the state of NGN and DHN, the dynamic energy flow models in gas and heat network are introduced in Sects. 3.3 and 3.4, respectively. Finally, a united dynamic energy flow problem with VSB model is formulated in Sect. 3.5.

3.1 The power flow formulation with proposed VSB model

The power flow analysis with VSB model reclassifies the bus into four types, which are reference, virtual slack, voltage-controlled and load buses. The reference bus, voltage-controlled bus (PV model) and load buses (PQ model) are consistent with the traditional power flow analysis. The virtual slack buses are mainly acted by energy conversion units with adjustable active power, which can be considered as voltage-controlled and load buses with variable active power, respectively. Thus, the specific bus types of ECUs under different operating conditions are subdivided as follows:

(1) Participating generators ($\widetilde{P}V$ bus model);

(2) participating negative generators ($\widetilde{P}Q$ bus model);

(3) non-participating generators (PV bus model);

(4) non-participating negative generators (PQ bus model), where $\widetilde{P}V$ bus has following characteristics: 1) The generation active power P_i is adjustable with each iteration. 2) The magnitude of voltage V_i is specified. 3) The phase angle of voltage θ_i is unknown. $\widetilde{P}Q$ bus has following characteristics: 1) The consumption active power P_i is adjustable with each iteration. 2) The magnitude of voltage V_i is unknown. 3) The phase angle of voltage θ_i is unknown. When all the ECUs quit participating active power adjustment due to the capacity or operation limit, the VSB type $\widetilde{P}V$ or $\widetilde{P}Q$ degenerate into traditional bus type PV or PQ.

Finally, the power balance equations for power flow analysis based on the new node types are given by

$$\Delta P_i = P_i^{\mathrm{vsb}} + P_i^{sp} - \sum_{j=1}^{N_e} P_{ij}, \quad \forall i = 1, \cdots, N_{\widetilde{P}V} + N_{\widetilde{P}Q}, \tag{12}$$

$$\Delta P_i = P_i^{sp} - \sum_{j=1}^{N_e} P_{ij,} \quad \forall i = (N_{\widetilde{P}V} + N_{\widetilde{P}Q} + 1), \cdots, N_e - 1, \tag{13}$$

$$\Delta Q_i = Q_i^{sp} - \sum_{j=1}^{N_e} Q_{ij}, \quad \forall i = 1, \cdots, (N_e - N_{\widetilde{P}V} - N_{PV} - 1), \tag{14}$$

where P_i^{sp} and Q_i^{sp} are the specific active and reactive power values injected into bus i, respectively. $N_{\widetilde{P}V}$, $N_{\widetilde{P}Q}$ and N_{PV} are the number of $\widetilde{P}V$, $\widetilde{P}Q$ and PV buses, respectively. $\sum_{j=1}^{N_e} P_{ij}$ and $\sum_{j=1}^{N_e} Q_{ij}$ are the power transmitted in the line, represented by the second term in right-hand side of eqs. (1) and (2).

3.2 The energy conversion units (ECUs) model

The energy conversion between the subnetworks occurs in CHP [14], GPG [5,13,14], P2G [5,22], EB units [23], which are modeled as follows:

$$M_{g,i}^{\mathrm{CHP}} = \frac{\rho_g}{\mathrm{GCV}_i}\left(\frac{P_i^{\mathrm{CHP}} + c_m P_i^{\mathrm{CHP}}}{\eta_{\mathrm{CHP}}}\right), \tag{15}$$

$$M_{g,i}^{\mathrm{GPG}} = \frac{\rho_g}{\mathrm{GCV}_i}(k_\alpha (P_i^{\mathrm{GPG}})^2 + k_\beta P_i^{\mathrm{GPG}} + k_\gamma), \tag{16}$$

$$M_{g,i}^{\mathrm{P2G}} = \frac{\rho_g \eta_{\mathrm{P2G}}}{\mathrm{GCV}_i} P_i^{\mathrm{P2G}}, \tag{17}$$

$$P_i^{\mathrm{EB}} = \frac{C_p M_h (T_{s,i} - T_{r,i})}{\eta_{\mathrm{EB}}}, \tag{18}$$

where eqs. (15) and (16) represent the relationship between the consumed gas flow M_g^{CHP} and M_g^{GPG} and generated active power of CHP and GPG units, respectively. c_m is the heat-to-power ratio of CHP [24]. k_α, k_β and k_γ are the heat rate coefficients of GPG. η_{CHP}, η_{P2G} and η_{EB} are the energy conversion efficiency of CHP, P2G and EB units, respectively. ρ_g and GCV are the density and gross calorific value of natural gas. Note the units of GCV and ρ_g are MJ/m^3 and kg/m^3, respectively. Thus, the obtained $M_{g,i}$ is kg/s. Eq. (17) gives a universal formula to express the relationship between consumed power P_i^{P2G} and generated gas flow $M_{g,i}^{\mathrm{P2G}}$ of P2G units. For EBs, electricity is consumed to generate heat power as is shown in eq. (18). $T_{s,i}$ and $T_{r,i}$ are the supply and return temperature of EB. M_h is the mass flow in DHN.

3.3 Dynamic energy flow model in natural gas network

The gas fluid dynamics are specified by one-dimensional partial differential equations (PDEs) including material-balance equation and the momentum equation, as is shown below:

$$\frac{\partial \Pi}{\partial t}+\frac{4c^2}{\pi D_g^2}\frac{\partial M_g}{\partial x}=0, \tag{19}$$

$$\frac{\partial \Pi}{\partial x}+\frac{4}{\pi D_g^2}\frac{\partial M_g}{\partial t}+\frac{\partial(\rho_g u)^2}{\partial x}+\frac{8fc^2}{\pi^2 D_g^5}\frac{M_g\left|M_g\right|}{\Pi}=0. \tag{20}$$

To obtain the numerical solutions of PDEs, the numerical method based on implicit trapezoidal rule to approximate gas dynamics can be found in ref. [25]. Then, the numerical formulations for a pipeline related to time and space segments are given by

$$\frac{\Pi_{x+1}^{t+1}-\Pi_{x+1}^{t}}{2\Delta t_g}+\frac{\Pi_{x}^{t+1}-\Pi_{x}^{t}}{2\Delta t_g}+\frac{4c^2(M_{g\,x+1}^{t+1}-M_{g\,x}^{t+1})}{\pi D_g^2\Delta x_g}=0, \tag{21}$$

$$\begin{aligned}&\frac{\Pi_{x+1}^{t+1}-\Pi_{x}^{t+1}}{\Delta x_g}+\frac{2(M_{g\,x+1}^{t+1}-M_{g\,x+1}^{t})}{\pi D_g^2\Delta t_g}+\frac{2(M_{g\,x}^{t+1}-M_{g\,x}^{t})}{\pi D_g^2\Delta t_g}\\&=\frac{fu_0^2}{4c^2D_g}(\Pi_{x+1}^{t+1}-\Pi_{x}^{t+1})-\frac{2fu_0}{\pi D_g^3}(M_{g\,x+1}^{t+1}-M_{g\,x}^{t+1}),\end{aligned} \tag{22}$$

where Δt_g and Δx_g are the temporal and spatial step size, respectively. Π and M_g represent the gas pressure and mass flow rate varying with time and space, respectively. c and u_0 are the speed of sound and reference gas flow velocity. D_g and f are the diameter and friction factor of the pipeline.

The calculating results are depended on the time and space step size Δt_g and Δx_g. In addition, the boundary conditions of eqs. (21) and (22) need to be set at the ends of pipelines to obtain a definite solution, including flow and pressure. The nodal outflow of node i is updated by

$$M_{g,i}=M_{g,i}^{L}+M_{g,i}^{\mathrm{CHP}}+M_{g,i}^{\mathrm{GPG}}-M_{g,i}^{\mathrm{P2G}}, \tag{23}$$

where $M_{g,i}^{L}$ is the gas load flow.

Assuming that the pipelines $k_1, k_2, ..., k_n$ are connected and intersect at node i, the mass flow into and out of node i should be balanced, and the pressure should be equal, as shown

$$\frac{M_{g,i}^{\mathrm{out}}}{A_j}=\frac{M_{g,k_1}^{\mathrm{end}}}{A_{k_1}}+\frac{M_{g,k_2}^{\mathrm{end}}}{A_{k_2}}+\cdots+\frac{M_{g,k_n}^{\mathrm{end}}}{A_{k_n}}, \tag{24}$$

$$\Pi_{k_1}^{\mathrm{end}}=\Pi_{k_2}^{\mathrm{end}}=\cdots=\Pi_{k_n}^{\mathrm{end}}, \tag{25}$$

where A_j is the cross-sectional area of pipeline j with node i as the sending node; A_{k_i} is the cross-sectional area of pipeline k_i; $\Pi_{k_i}^{\mathrm{end}}$ is the pressure at the end of the pipeline k_i.

3.4 Dynamic energy flow model in district heating network

The temperature dynamic along the pipeline is focused in district heating network. Similarly, the dynamic is specified by one-dimensional PDE related to time and space.

$$A_h\rho_h C_p\frac{\partial T}{\partial t}+C_pM_h\frac{\partial T}{\partial x}=\frac{1}{R}(T_a-T), \tag{26}$$

where T is the temperature variable in DHN, T_a is the environment temperature, A_h and R are the cross section area and thermal resistance of DHN pipeline, ρ_h and C_p are the density and specific heat capacity of water.

In order to get the numerical solutions of eq. (26), a characteristic line method with superior computational efficiency to approximate temperature dynamic can be found in ref. [26]. In this method, the temperature T_i^{t+1} is calculated by the third order Lagrange interpolation polynomial with temperature T_{i-2}^{t}, T_{i-1}^{t}, T_i^{t} and T_{i+1}^{t} at the previous temporal step. The final numerical formulation related to time and space segments is given by

$$\begin{aligned}T_i^{t+1}=k\Delta t_hT_a+(1-k\Delta t_h)\Bigg[&\frac{(\Delta x_h-\alpha)\alpha(\alpha+\Delta x_h)}{-6\Delta x_h^3}T_{i-2}^{t}\\&+\frac{(2\Delta x_h-\alpha)\alpha(\alpha+\Delta x_h)}{2\Delta x_h^3}T_{i-1}^{t}\\&+\frac{(2\Delta x_h-\alpha)(\Delta x_h-\alpha)(\alpha+\Delta x_h)}{2\Delta x_h^3}T_{i}^{t}\\&+\frac{(2\Delta x_h-\alpha)\alpha(\Delta x_h-\alpha)}{6\Delta x_h^3}T_{i+1}^{t}\Bigg],\end{aligned} \tag{27}$$

where $k=1/(A_c\rho_hC_pR)$, $\alpha=M_h\Delta t_h/(\rho_hA_c)$, Δt_h and Δx_h are the temporal and spatial step size of heat network. M_h operate with rated mass flow rate to maintain stable hydraulic conditions [27]. The solution of eq. (27) needs to combine the temperature boundary conditions. The supply temperature at source node and return temperature at sink node are generally known as $T_{S,i}^{0}$ and $T_{R,i}^{0}$. The mixed temperature at nodes receiving water flow from multiple pipelines or nodes is unknown, which is calculated by

$$T_{i,\mathrm{mix}}=\frac{\sum T_{k_{\mathrm{end}}}^{\mathrm{in}}M_{h,k}+\sum T_i^{\mathrm{in}}M_{h,i}}{\sum(M_{h,k}+M_{h,i})}, \tag{28}$$

where $M_{h,k}$ is the water flow from pipeline k into node i; $T_{k_{\mathrm{end}}}^{\mathrm{in}}$ represents the temperature at the terminal spatial segment of pipeline k; $M_{h,i}$ is the flow injected into node i by source in supply network, or injected into node i by load in return network. T_i^{in} is the temperature of $M_{h,i}$.

3.5 Flowchart of integrated energy flow algorithm

The flowchart in Figure 1 summarizes the steps of the integrated energy flow with proposed VSB model. In the stage 1, the power generations at virtual slack buses are determined based on the calculated power sensitivity matrix for adaptive sharing power among generators. Then, the VSB power flow

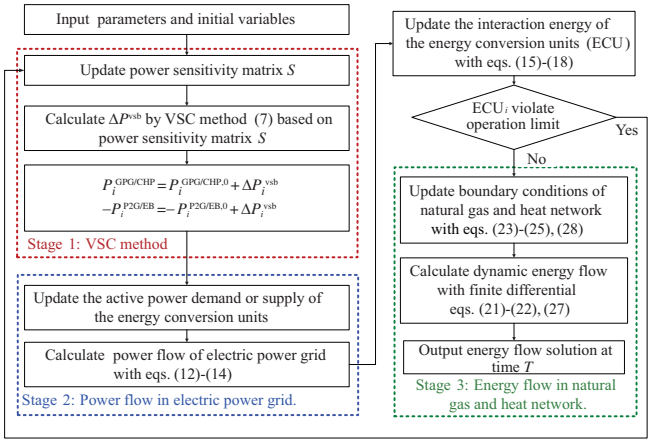

Figure 1 Flowchart of the united energy flow solution.

is re-established in stage 2, which is used to compensate the power deviations. Next, if the energy conversion unit violates its operating limits, node type will be re-defined and power sensitivities will be updated with the new system conditions. Then, the calculated energy interaction values of the conversion units are given to heat or gas network to update their boundary conditions. Finally, the impacts of VSB model on natural gas and heat network are obtained in stage 3.

In summary, the proposed VSB model based on the power sensitivity adaptively realizes the power sharing when power fluctuates. The method combines the advantages of the energy conversion unit, and balances the power of EPG with the help of the NGN and DHN.

4 Case studies

In this section, proposed VSB model and its energy flow analysis will be tested. For the first case study, a 24-bus power system is utilized to demonstrate the implement and show the effect of the proposed model. For the second case study, a much larger system consisting of electric, natural gas and district heating network is used to show the effects of VSB model on integrated energy system.

4.1 An illustrative case with VSB model

The effectiveness of VSB model is verified by the simulation of 24-bus power system [28], as is shown in Figure 2. In this electric network, five sets of ECUs are located at bus E2, E15, E16, E18 and E21, respectively, which are defined as virtual slack buses. A slack generator is located at bus E1 (i.e. single reference bus). To show the performance of proposed VSB model, we compare it with two typical methods: 1) single slack bus (SSB) model in ref. [5]; 2) distributed slack bus (DSB) model mentioned in refs. [9, 13, 14]. A set of load changes are presented to simulate power mismatches to compare the performance of several models in power balancing. As is shown in Figure 3, the load at each bus increases in turn.

For the SSB and DSB, the active power outputs of electric generators are regulated based on their assigned participation factors, which are reported in Table 1. For the proposed VSB model, the active power values of ECUs are determined based on the power sensitivities, which are given in Figure 4.

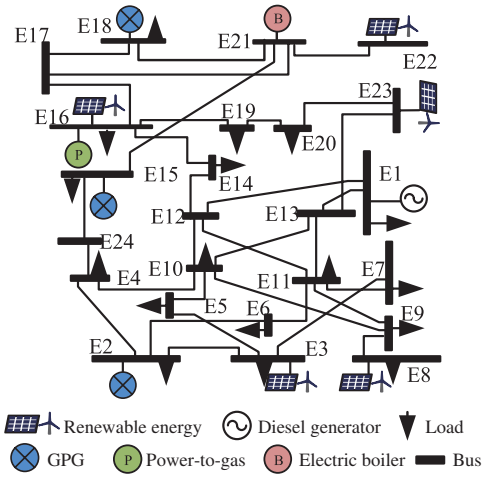

Figure 2 Schematic diagram of the test system in Sect. 4.1.

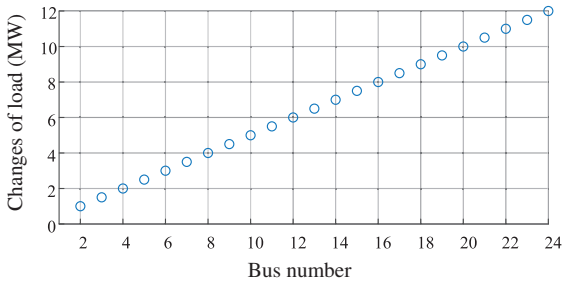

Figure 3 The load changes in the 24-bus power system.

Table 1 Participation factors of electric generators

Buses	SSB	DSB
1	1.0	0.2
2	0.0	0.5
15	0.0	0.2
18	0.0	0.1

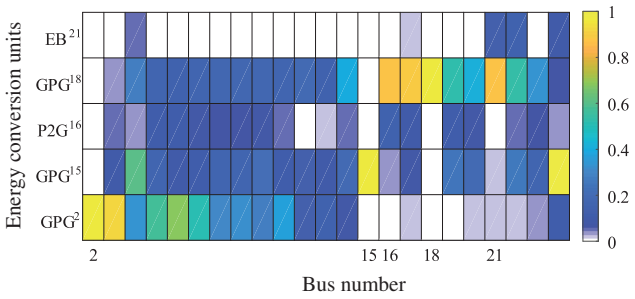

Figure 4 Power output or input of energy conversion units (MW).

Figure 4 shows the power sensitivities relationship between the ECUs and power fluctuations in each bus. The different value of power sensitivity is represented by the heatmap with different color, where the highest sensitivity with the amount of 1 is represented by bright yellow, while zero sensitivity is represented by white. For instance, the power fluctuations at bus E2, E15, E18 are controlled by the corresponding ECUs with the highest sensitivity of 1.

Figure 5 gives the power output of the single slack generator with different models. For the SSB model (blue bar), all the participation factors of generators at non-slack buses are zeros. Thus, the total load and power losses of the power system are balanced by the only slack generator. It can be seen that when the load increases by 12 MW, the generator output increases from 23.2 to 35.3 MW. The increment of the generator output power is approximately equal to the increment of the load. It can also be proved from the outputs of ECUs in Figure 6(a). All ECUs output constant power and generate or consume powers regardless of load variations. For the DSB model (red bar), the active power output of reference bus is significantly lower than that in SSB model. This is because the several electric generators work together as slack buses to balance active power changes. It can be seen from Figure 6(b) that the GPG^{2} unit connected to bus 2 plays a main regulating role, which is consistent with the participation factors. However, due to the constant participation factors, each generator cannot adjust its active power output flexibly according to the position and amount of load changes. The GPG^{2} loses its regulating ability because of the capacity limit when the load changes increase by 8 MW, while the other units still operate at the original participation factor. After that, the power output of reference bus increases because the additional power changes are still balanced by the single reference bus.

For the VSB model (orange bar), the load changes are shared together with all ECUs. The power outputs in each ECU are shown in Figure 6(c). It can be seen that the load changes at bus E2, E15 and E18, are mainly balanced by the power generation of GPG unit at corresponding buses, which is consistent with their highest power sensitivities (shown in Figure 4). The power fluctuations at buses E16 and E21 are controlled by the corresponding ECUs with lower sensitivity. This is because the ECUs at the buses reach their operating limit and do not participate in power regulation thereafter. Hence, the power fluctuations at buses E16 and E21 are compensated by several units. For instance, the power changes at E16 are mainly balanced by GPG^{18} and $P2G^{16}$. Their power sensitivities are represented by yellow (with the value of 0.8438) and blue (with the value of 0.1522), respectively. Thus, the power output of bus E18 is increased by 6.75 MW and the power input of bus E16 is decreased by 1.22 MW, respectively, as is shown in Figure 6(c). Similarly, for the buses which are not directly connected with ECU, the power fluctuations at the buses are compensated by several units based on the sensitivity.

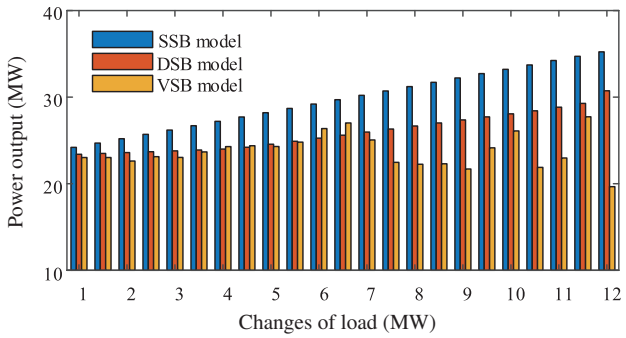

Figure 5 The power sensitivity relationship between the ECUs (the superscript is the number of electric bus) and the power fluctuations at different electric bus.

Therefore, the proposed VSB method is helpful to reduce the burden of single slack generator. The utilization of ECUs with power adjustment can effectively address overload and accommodate more power fluctuations.

4.2 The effect of VSB model on dynamic energy flow results

In this case, the integrated IEEE 57-bus power system [1)], Belgian 20-node gas system [29] and a modified 14-node radial heat network [14] are used, as is shown in Figure 7. The connections between the subnetworks and the ECUs are shown in Table 2. The CHP unit is installed at bus E1 as the reference bus, and other ECUs are used as the virtual slack bus. The conversion efficiency of CHP, P2G and EB are η_{CHP} = 0.895, η_{P2G} = 0.7, η_{EB} = 0.95, respectively. The heat rate coefficients of GPG units are k_{α}=0.01, k_{β}=4, γ=150. Other considered parameters are as follows: GCV = 40.14 MJ/m^3, ρ_g=0.725 kg/m^3, c_m=1.266; C_p=4182 J/kg·K, c=380 m/s, u_0 = 10 m/s, ρ_h = 960 kg/m^3. The step sizes of NGN and DHN are $\Delta t_g = \Delta t_h$ = 30 s, Δx_g=500 m, Δx_h = 1000 m.

4.2.1 The effect of using VSB model on energy flow results

To investigate the impact of balancing power with the VSB model on the total integrated electric-gas-heat system, stochastic wind power and power demand measured at hourly intervals are injected into the electric network, as is shown in Figure 8(a). The data in one week are obtained from Energinet.dk, the power transmission system operator in Denmark. The stochastic wind power is injected into node E2 and node E9, respectively. The time-series of power demand

1) The standard IEEE 57-bus test system. University of Washington. Available: http://www.ee.washington.edu/research/pstca/, 2022

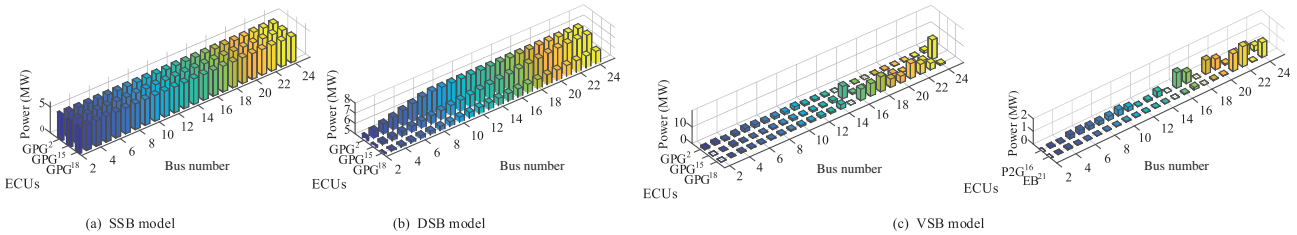

(a) SSB model (b) DSB model (c) VSB model

Figure 6 Power output of diesel generation (MW).

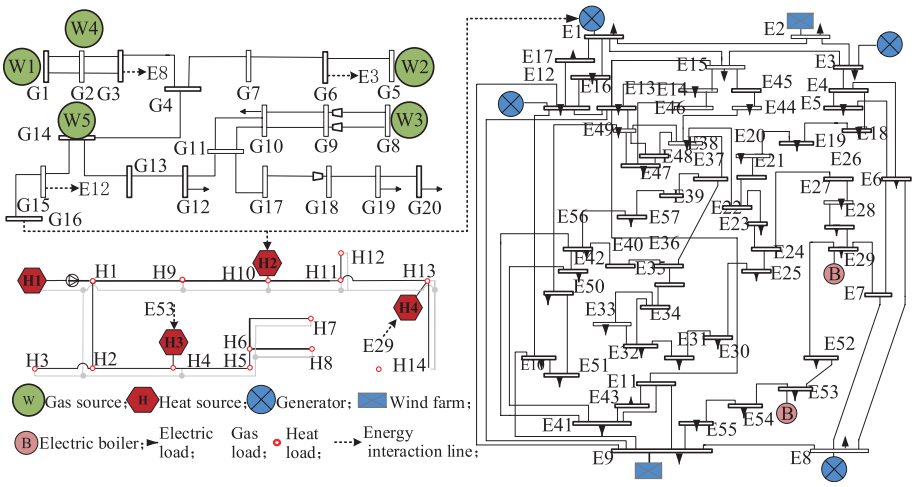

Figure 7 Schematic diagram of the test system in Sect. 4.2.

Table 2 Connection of units between the subnetworks in Case 2

Energy conversion units	Electric bus	Gas node	Heat node
CHP	1	16	10
Gas-fired power generator	3	6	–
Gas-fired power generator	8	3	–
Gas-fired power generator	12	15	–
Power-to-gas	33	2	–
Power-to-gas	47	14	–
Electric boiler	29	–	13
Electric boiler	53	–	4

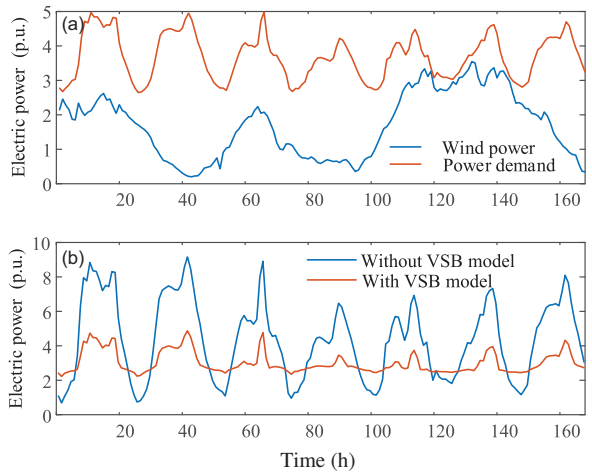

Figure 8 The fluctuation of power demand and wind power.

is injected into electric network through all load nodes, respectively.

The different energy flow results with VSB and without VSB model are analyzed from the following aspects: 1) the active power output of reference bus; 2) voltage profile; 3) pressure profile; 4) temperature profile.

1) The Active Power Output of Single Reference Bus: Figure 8(b) shows the active power output of the reference bus. The case with VSB method reduces the active power supplied by the reference bus when power demand increases, and has a maximum 54.3% reduction compared with the result without VSB method. Furthermore, if the capacity of reference bus is limited to 8 p.u, the system would overload without without VSB method. But when the power demand decreases, the output power of reference bus in VSB is generally higher than that without VSB. This is because when the power demand fluctuates downward or renewable power fluctuates upward, the units such as GPG decrease their output, while P2G and EB increase their consumption based on the power sensitivity as is shown in Figure 9. In conclusion, the VSB method can help reduce the burden of reference bus, and has a potential to decrease the wind curtailment.

2) Voltage Profile: Figure 10 shows the voltage magnitude and phase angle at the buses which are away from the generator buses. It can be found that the voltage profile with the VSB (Figure 10(b) and (d)) is higher than that without VSB

(Figure 10(a) and (c)). The voltage magnitude and phase angle with VSB model are increased by 0.02 p.u. and 2.24 degree, respectively. Meanwhile, the voltage results with VSB fluctuate in a smaller range than those without VSB. This is because, for the results with VSB model, the active power change in Figure 8 is shared by multiple energy conversion units. Then, the generation unit at reference bus does not need to transmit long distance to maintain power balance. It is also proved by the results of power losses in Figure 11, that the fluctuation range of power loss from 0.496 to 0.766 p.u. without VSB, is reduced within 0.499–0.717 p.u. with VSB. This is because in a normal condition, the larger voltage differences cause the larger current resulting in power losses [19].

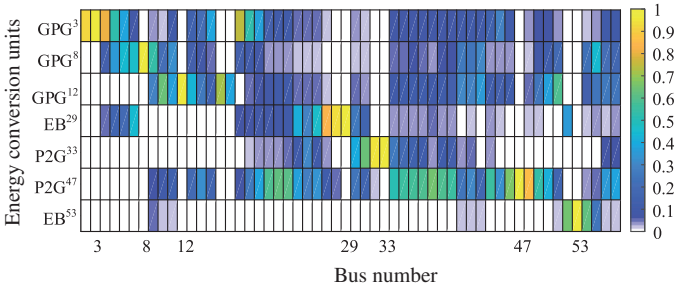

Figure 9 The power sensitivity relationship between the energy conversion units (the superscript is the number of electric bus) and the power fluctuations.

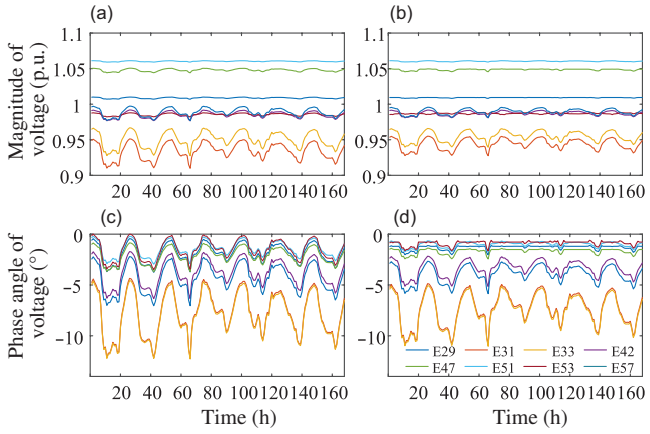

Figure 10 Magnitude of voltage (a) without the VSB, and (b) with the VSB; phase angle of voltage (c) without the VSB, and (d) with the VSB.

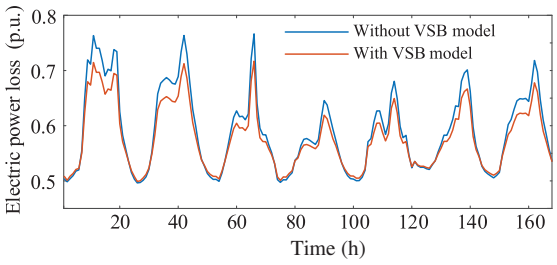

Figure 11 The power loss in integrated system with VSB versus without VSB.

3) Pressure Profile: Just like the voltage is an important factor for electricity network, the pressure is an important factor for the safety of gas network. Figure 12 shows the pressure profile at the ends of gas network and coupling nodes. It can be found that the results without proposed VSB (Figure 12(a)) have a lower pressure profile and a larger fluctuation range than those of with VSB (Figure 12(b)). This is because in the model VSB, all the power fluctuations of electric network are balanced by the single CHP installed at node G16 of gas network, which leads to a larger fluctuation range of flow demand and pressure at G16. On the contrary, in the model with VSB, the gas demand at G16 is jointly shared by GPG units at G3, G6 and G15. Then, the burden of G16 is reduced and the corresponding pressure fluctuates in a smaller range. It is worth noting that the maximum pressure difference is at the terminal of gas network, node G20. The value of the pressure difference is 13.952 bar at most, which is increased by 167.4%. The comparison indicates that the use of VSB method not only reduces the active power output of the reference bus, but also greatly reduces the burden of gas network for power balancing, which is more helpful for the reliable operation for gas network of IES.

4) Temperature Profile: The temperature is a reflection of the heat network and the coupling units behavior. Figure 13(a) and (b) shows the nodal supply temperature results without and with VSB model, respectively. In this simulation, the use of VSB model makes the temperature variation range of node H4, H13 and their nearby nodes become larger. According to ref. [27], a higher supply temperature has a larger heat loss. Hence, the thermal power loss has a larger fluctuation range in the results with VSB model, as is shown in Figure 14.

4.2.2 *The dynamic process of IES*

To demonstrate the effect of the dynamic model on final energy flow results, two energy flow calculation methods are compared: 1) the dynamic energy flow calculation in this

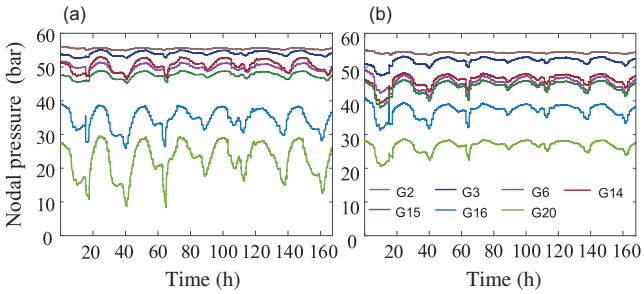

Figure 12 Nodal pressure (a) without the VSB, and (b) with the VSB.

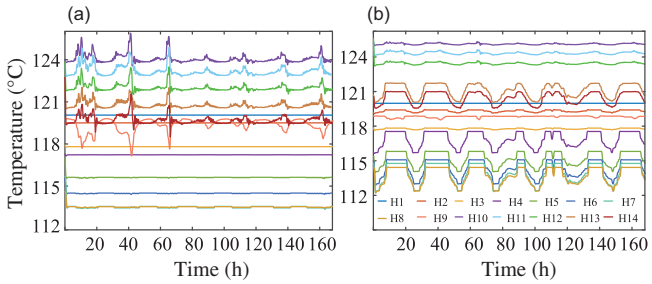

Figure 13 Nodal supply temperature (a) without VSB model, and (b) with VSB model.

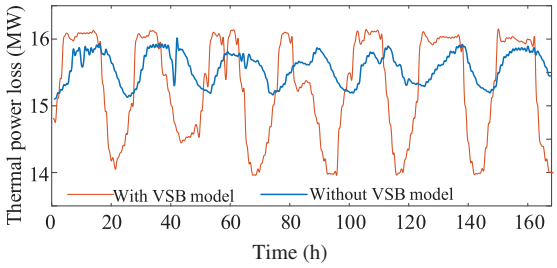

Figure 14 Thermal power loss of heat network.

paper; 2) traditional steady-state energy flow calculation. Taking a one hour change of electric load as an example, the dynamic processes of IES before and after the load change are analyzed. Table 3 shows the operational state changes of IES. The detailed partial dynamic process results comparisons between two methods of gas pipelines and heat pipelines are presented in Figures 15 and 16.

The supply temperature change processes of heat pipelines connected to CHP node are shown in Figure 15. For the dynamic EFC, as the heat power output of CHP units decreases (shown in column 4 of Table 3), the supply temperature of H10 decreases at time 1 h (shown in Figure 15(a)). Next, the supply temperature of H11 at terminal of pipe H10-H11 also decrease and enter a new steady state at about 1.5 h (shown in Figure 15(c)). Note that the temperature of H9 (shown in Figure 15(a)) starts to increase around 1.5 h, as the slack node H1 increases its output in response to the heat power shortfall of CHP at node H10. Correspondingly, the water with more heat energy flows from slack node to node H9, and then, the temperature fluctuation spreads from node H9 to H10 and H11. Finally, the supply temperature of node H10 and H11 increase and reach another new steady state after about 3.5 h. For the steady-state EFC (shown in Figure 15(b) and (d)), the results are only represented by several discrete points to shown the trend. There is no dynamic process, and all temperature values change at the same time after the network state changes, leading to a lot of dynamic information missing.

The dynamic gas flow and pressure change processes of gas pipelines connected to CHP node are compared in Figure 16. The decrease of gas flow consumed by CHP unit at G16

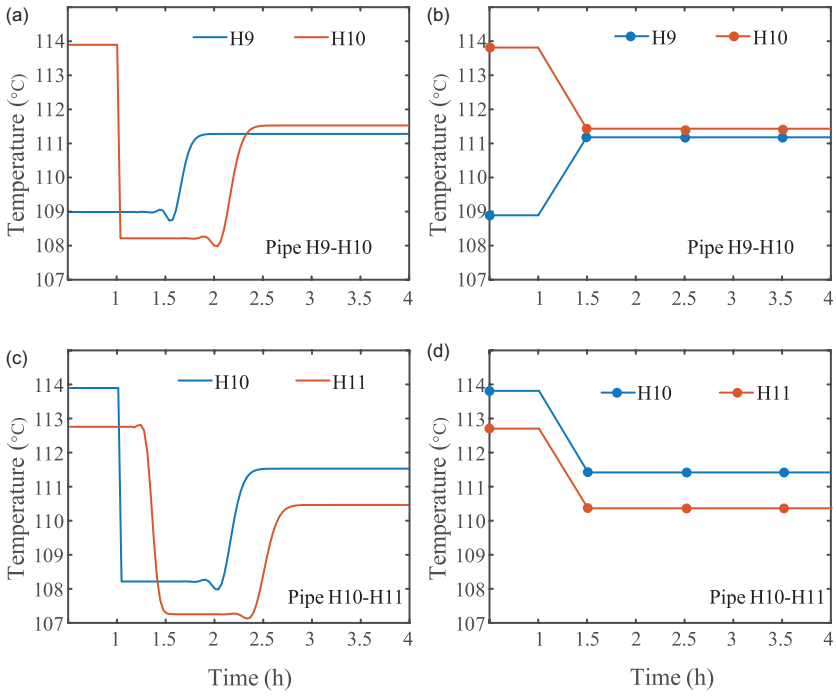

Figure 15 The dynamic process of supply temperature of (a) pipelines 9 and 10, and (c) pipelines 10 and 11. The steady-state supply temperature of (b) pipelines 9 and 10, and (d) pipelines 10 and 11.

Table 3 The operating state changes of IES

Period	P^{load} (MW)	P^{CHP} (MW)	H^{CHP} (MW)	H^{slack} (MW)	M^{CHP} (kg/s)
t_0	124.25	40.22	50.28	123.39	1711.8
t_1	107.45	21.04	26.30	147.36	894.6

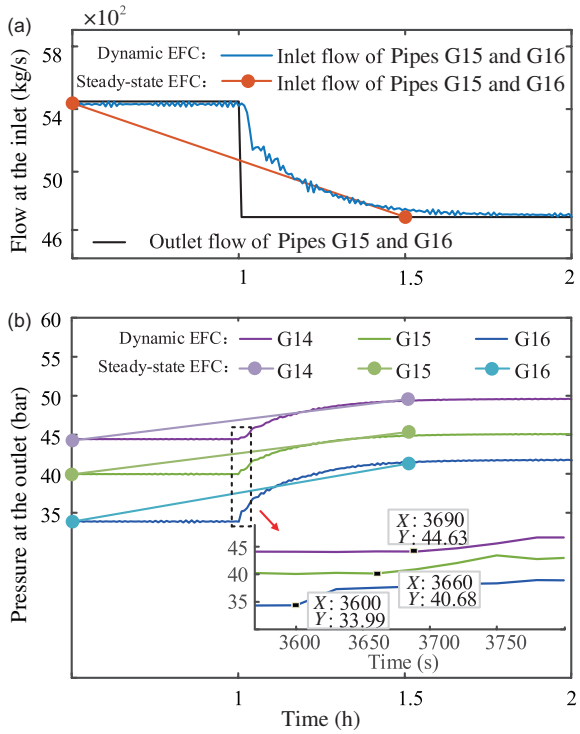

Figure 16 (a) The mass flow at the inlet of pipelines; (b) the pressure at the outlet of pipelines.

causes a difference between the inlet flow and outlet flow of pipeline 15 and 16. Then, the pressure wave responds firstly, causing slow decrease of the inlet flow of pipeline 15 and 16. It can be seen from Figure 16(a), the gas flow reaches a new steady state about an hour later in the dynamic EFC, while the inlet flow change is only represented by two discrete points in the steady-state EFC. The pressure changes sequentially along pipelines. As is shown in Figure 16(b), the pressure at node G16 starts to change at 3600 s. Meanwhile, node G15 and node G14 change at 3660 and 3690 s, respectively. The results obtained by steady-state EFC are discrete values, marked with dots to show the trend. This trend is consistent with dynamic EFC, but there is no dynamic process.

In brief, the dynamic energy flow calculation method considers the state variables over time, while the latter does not. The dynamic EFC has better characteristics of reflecting both heat and gas dynamic process, which offers more intact and comprehensive information for the subsequent optimization and control of IES.

5 Conclusions

This paper had proposed the network-based virtual-slack bus (VSB) model for the electric power grid in integrated energy system (IES). Based on the power sensitivity analysis method, the model was implemented by making full use of the advantage of energy conversion units (ECUs) in adjusting power to balance power. To implement the proposed VSB model, the dynamic energy flow analysis had been established to realize the system state assessment of IES and stable operation analysis. Several case studies had been carried out. With VSB model, the power imbalances caused by changes of load or renewable were adaptively shared by the ECUs based on their power sensitivities. Moreover, the burden of power balancing of single reference bus and the primary energy side gas network were both reduced, which is helpful to address the limited capacity problem and accommodate more power fluctuation. Furthermore, the voltage profile of electric power grid and pressure profile of gas network are maintained when the power fluctuate. Therefore, the proposed network-based VSB method is expected to integrate a high penetration of renewable energy into electric power grid, especially the grid operating in coupled mode in the context of dual carbon.

This work was supported by the National Key Research and Development Program of China (Grant No. 2018YFA0702200), the National Natural Science Foundation of China (Grant Nos. U20A20190 and 62073065), and the Fundamental Research Funds for the Central Universities in China (Grant No. N2204003).

1 Zhao X, Ma X, Chen B, et al. Challenges toward carbon neutrality in China: Strategies and countermeasures. Resour Conserv Recycl, 2020, 176: 105959
2 Wang Y, Zhang J Y, Zhao Y C, et al. Exergy life cycle assessment model of "CO_2 zero-emission" energy system and application. Sci China Tech Sci, 2011, 54: 3296–3303
3 Xi L, Yu L, Zhang X, et al. Automatic generation control of ubiquitous power Internet of Things integrated energy system based on deep reinforcement learning (in Chinese). Sci Sin Tech, 2020, 50: 221–234
4 Wu H F, Zhang B W, Qu W J, et al. Integration of a thermochemical energy system driven by solar energy and biomass for natural gas and power production. Sci China Tech Sci, 2022, 65: 1383–1395
5 Zeng Q, Fang J, Li J, et al. Steady-state analysis of the integrated natural gas and electric power system with bi-directional energy conversion. Appl Energy, 2016, 184: 1483–1492
6 Cai N, Khatib A R. A universal power flow algorithm for industrial systems and microgrids-active power. IEEE Trans Power Syst, 2019, 34: 4900–4909
7 Exposito A G, Ramos J L M, Santos J R. Slack bus selection to minimize the system power imbalance in load-flow studies. IEEE Trans Power Syst, 2004, 19: 987–995
8 Tong S, Miu K N. A network-based distributed slack bus model for DGs in unbalanced power flow studies. IEEE Trans Power Syst, 2005, 20: 835–842
9 Ortega J, Molina T, Muñoz J C, et al. Distributed slack bus model formulation for the holomorphic embedding load flow method. Int Trans Electr Energ Syst, 2020, 30: e12253
10 Kamh M Z, Iravani R. A sequence frame-based distributed slack bus

model for energy management of active distribution networks. IEEE Trans Smart Grid, 2012, 3: 828–836
11 Chertkov M, Backhaus S, Lebedev V. Cascading of fluctuations in interdependent energy infrastructures: Gas-grid coupling. Appl Energy, 2015, 160: 541–551
12 Qiao Z, Guo Q, Sun H, et al. An interval gas flow analysis in natural gas and electricity coupled networks considering the uncertainty of wind power. Appl Energy, 2017, 201: 343–353
13 Martinez-Mares A, Fuerte-Esquivel C R. A unified gas and power flow analysis in natural gas and electricity coupled networks. IEEE Trans Power Syst, 2012, 27: 2156–2166
14 Shabanpour-Haghighi A, Seifi A R. An integrated steady-state operation assessment of electrical, natural gas, and district heating networks. IEEE Trans Power Syst, 2016, 31: 3636–3647
15 Hu Y, Lian H, Bie Z, et al. Unified probabilistic gas and power flow. J Mod Power Syst Clean Energy, 2017, 5: 400–411
16 Huang Y, Sun Q, Zhang N, et al. A multi-slack bus model for bi-directional energy flow analysis of integrated power-gas systems. CSEE J Power Energy Sys, 2022, doi: 10.17775/CSEE-JPES.2020.04190
17 Wu J, Yang X P. An area method for visualizing heat-transfer imperfection of a heat exchanger network in terms of temperature-heat-flow-rate diagrams. Sci China Tech Sci, 2016, 59: 1517–1523
18 Qin X, Sun H, Shen X, et al. A generalized quasi-dynamic model for electric-heat coupling integrated energy system with distributed energy resources. Appl Energy, 2019, 251: 113270
19 Choi D H, Park J W, Lee S H. Virtual multi-slack droop control of stand-alone microgrid with high renewable penetration based on power sensitivity analysis. IEEE Trans Power Syst, 2018, 33: 3408–3417
20 Chen X, Kang C, O'Malley M, et al. Increasing the flexibility of combined heat and power for wind power integration in China: Modeling and implications. IEEE Trans Power Syst, 2015, 30: 1848–1857
21 Sun Q, Dong Q, You S, et al. A unified energy flow analysis considering initial guesses in complex multi-energy carrier systems. Energy, 2020, 213: 118812
22 Qadrdan M, Abeysekera M, Chaudry M, et al. Role of power-to-gas in an integrated gas and electricity system in Great Britain. Int J Hydrogen Energy, 2015, 40: 5763–5775
23 Liu X. Combined analysis of electricity and heat networks. Dissertation for Doctoral Degree. Cardiff: Cardiff University, 2013
24 Liu X, Jenkins N, Wu J, et al. Combined analysis of electricity and heat networks. Energy Procedia, 2014, 61: 155–159
25 Liu W, Li P, Yang W, et al. Optimal energy flow for integrated energy systems considering gas transients. IEEE Trans Power Syst, 2019, 34: 5076–5079
26 Wang Y, You S, Zhang H, et al. Thermal transient prediction of district heating pipeline: Optimal selection of the time and spatial steps for fast and accurate calculation. Appl Energy, 2017, 206: 900–910
27 Yao S, Gu W, Lu S, et al. Dynamic optimal energy flow in the heat and electricity integrated energy system. IEEE Trans Sustain Energy, 2021, 12: 179–190
28 Beerten J, Cole S, Belmans R. Generalized steady-state VSC MTDC model for sequential AC/DC power flow algorithms. IEEE Trans Power Syst, 2012, 27: 821–829
29 De Wolf D, Smeers Y. The gas transmission problem solved by an extension of the simplex algorithm. Manage Sci, 2000, 46: 1454–1465